Structural damage detection and localization using changes in phase angle

Sherif Beskhyroun*, Shuichi Mikami**, and Toshiyuki Oshima***
シェリフ　ベスキロウン*, 三上修一**, 大島俊之***

*Doctoral Student, Dept. of Civil Eng., Kitami Institute of Technology, (165 Koen-cho, Kitami, 090-8507, Japan)
**Associate Professor, Dept. of Civil Eng., Kitami Institute of Technology, (165 Koen-cho, Kitami, 090-8507, Japan)
***Professor, Dept. of Civil Eng., Kitami Institute of Technology, (165 Koen-cho, Kitami, 090-8507, Japan)

A technique to detect and locate damage by measuring the vibration response of a structure is presented. The technique uses measured phase angle between two measuring channels from the healthy structure as reference data, and then monitors vibration measurements during the life of the structure to detect and locate the damage. The technique requires that the excitation forces used for the undamaged and damaged structure must have the same amplitude, location and waveform. The excitation force does not need to be measured and no structural model is needed. The proposed method is based on only the measured data without the need for any modal identification. The method is described theoretically and applied to the experimental data, from a steel bridge model and bookshelf structure. Several damage scenarios were introduced to the members of the test structures. The damage was detected and located accurately using the proposed method.

Key Words: Damage detection; Modal parameters; Health monitoring; Phase angle

1. Introduction

Most bridges or offshore structures are visually inspected for structural damage at specified regular intervals. However, this common nondestructive evaluation (NDE) method does not always reveal structural anomalies because many portions of the structure are not accessible to visual inspection and damage can propagate to critical levels between inspection intervals. Furthermore, this method does not provide a quantitative value for the remaining strength of the structure. Thousands of our aging bridges are overused and overloaded, and subsequently require structural repair. Rapid and efficient evaluation of structural health after hurricanes or earthquakes is highly desirable. These growing needs have motivated considerable research efforts to develop practical structural health monitoring systems[1, 2]. During the past two decades, numerous studies have addressed non-destructive damage evaluation via changes in the dynamic modal responses of a structure. All methods developed to date are classifiable into four levels according to their performance:[3, 4]

1. Level I – those methods that identify only whether damage has occurred.
2. Level II – those methods that identify whether damage has occurred and simultaneously determine the damage location.
3. Level III – those methods that identify whether damage has occurred, simultaneously determine the damage location, and further estimate the damage severity.
4. Level IV – those methods that identify if damage has occurred, simultaneously determine the damage location, estimate the damage severity, and assess the effect of that damage on the structure.

The level II non-destructive damage evaluation technique is performed in this study. Modal vibration data such as structural natural frequencies and mode shapes can characterize the state of the structure[5, 6]. This capability is attributable to the fact that damage in the form of changes in the structural physical properties (i.e., stiffness, mass, and boundary conditions) consequently alters such vibration properties of the structure as modal frequencies, mode shapes, and modal damping values[7]. Changes in the vibration properties can then serve as indicators of damage detection[8, 9].

Damage-detection methods such as acoustic or ultrasonic methods, magnetic field methods, radiograph, eddy-current methods and thermal field methods are either visual or localized experimental methods[10, 11]. Unfortunately, they are all localized techniques, implying long and expensive inspection time. The drawbacks of

current inspection techniques have led engineers to investigate new methods for continuous monitoring and global condition assessment of structures. That is the case for methods based on vibration responses that allow one to obtain meaningful time and/or frequency domain data and calculate changes in the structural and modal properties, such as resonance frequencies, modal damping and mode shapes. These properties are then used to develop reliable techniques to detect, locate and quantify damage[12]. Many damage detection schemes rely on analyzing response measurements from sensors placed on the structure[13, 14, 15, 16, 17]. Research efforts have been made to detect structural damage directly from dynamic response measurements in the time domain, e.g., the random decrement technique[18, 19], or from frequency response functions (FRF)[20]. Also, methods have been proposed to detect damage using system identification techniques[21, 22].

In this paper, a proposed algorithm based on changes in phase angle is presented. The technique requires that the excitation forces used for the undamaged and damaged structure must have the same amplitude, location and waveform in order to ensure that the changes in phase angle data are mainly due to damage and not due to the change in excitation force characteristics. The excitation force does not need to be measured. The algorithm is used to detect damage and locate its position using only the measured data without the need for any modal identification. The algorithm can also be used to monitor the damage growth but cannot be used to estimate the damage size or severity. The method is applied to the experimental data extracted from a steel bridge model after inducing some defects to its members. Releasing supporting bolts of some members introduced the damage to the bridge model. For further validation of the proposed method, it is also applied to the experimental data from a bookshelf structure. The damage in this case is introduced by releasing some bolts between the plates and columns of the bookshelf. The methodology can be applied in a similar manner to large civil engineering structures, such as steel bridges. For example, a number of sensors can be mounted on the main girder of the bridge to measure the acceleration response and a number of actuators can be used as a local excitation source for the main girder. The same excitation force (equal magnitude and the same waveform) can be produced for exciting the undamaged and damaged structure, as required to implement the damage identification technique presented in this paper. Undesired vibrations induced from wind, traffic or any other source can be avoided since the vibration data induced from the actuators can be generated at any desired time. Moreover, the traffic on the bridge does not need to be interrupted. The experimental models and type of damage presented here simulates the applicability of the method to steel structures. However, the implementation of the method to concrete structures is not investigated in this paper.

2. Theoretical description

Modal parameters such as mode shapes, resonant frequencies and damping are functions of the physical properties of the structure (mass, stiffness and boundary conditions). Damage will change the physical properties of the structure, which in turn will alter the modal parameters. Many techniques have been proposed in the area of non-destructive damage detection using changes in modal parameters. However, in many structures only few modes are available which may decrease the accuracy of detecting and localizing damage using these techniques. The basic premise of the proposed damage identification technique is that for each modal response the amplitude and phase angle can be estimated. Then, any change in the modal response due to the occurrence of damage will in turn change both the amplitude and the phase angle. In order to overcome the problem of the limited number of identified modal parameters, phase information estimated from the various accelerometer readings at all frequencies in the measurement range and not just the modal frequencies will be compared before and after damage using the proposed method. In order to identify the damage with more confidence, every measuring channel will be used once as a reference for other channels, which will create large sets of data. These sets of data can then be analyzed using statistical procedures to determine the damage location with more confidence, as will be explained in details in the following section.

Let $G_{xy}(f)$ denote the Cross Spectral Density (CSD), relating two time histories, x(t) and y(t). The phase angle between x and y can be computed from the real and imaginary values of G_{xy} as:

$$P_{xy}(f) = \tan^{-1}\left[imag(G_{xy}(f))/real(G_{xy}(f))\right]. \quad (1)$$

The absolute difference in absolute phase angle before and after damage can then be defined as

$$\Delta_{xy}(f) = \left\| P_{xy}(f) \right| - \left| P^{*}_{xy}(f) \right\| \quad (2)$$

where $P_{xy}(f)$ and $P_{xy}^{*}(f)$ represent the phase angle of the undamaged and damaged structures respectively. When the change in phase angle is measured at different frequencies on the measurement range from f_1 to f_m, a matrix $[\Pi_r]$ can be formulated as follows

$$\Pi_r = \begin{bmatrix} \Delta_{1r}(f_1) & \Delta_{1r}(f_2) & \cdots\cdots & \Delta_{1r}(f_m) \\ \Delta_{2r}(f_1) & \Delta_{2r}(f_2) & \cdots\cdots & \Delta_{2r}(f_m) \\ \cdot & \cdot & \cdots\cdots & \cdot \\ \cdot & \cdot & \cdots\cdots & \cdot \\ \cdot & \cdot & \cdots\cdots & \cdot \\ \Delta_{nr}(f_1) & \Delta_{nr}(f_2) & \cdots\cdots & \Delta_{nr}(f_m) \end{bmatrix}_r \quad (3)$$

where n represents the number of measuring points and r represents the number of reference channel. In matrix $[\Pi_r]$, every column represents the changes in phase angle at different measuring channels but at the same frequency value. Each measuring channel will be used as a reference for the other channels ($r = 1 : n$). Therefore, the matrix $[\Pi_r]$ will be formulated n different times (3D matrix). The summation of phase angle changes over different frequencies using different references can be used as the indicator of damage occurrence. In other words, the first damage indicator is calculated from the sum of rows of each matrix, $[\Pi_r]$ and then summing up these changes over different references

$$Total\_Change = \sum_r \begin{Bmatrix} \sum_f \Delta_{1r}(f) \\ \sum_f \Delta_{2r}(f) \\ \cdot \\ \cdot \\ \cdot \\ \sum_f \Delta_{nr}(f) \end{Bmatrix}_r \quad (4)$$

where $f = f_1 : f_m$ and $r = 1 : n$.

This indicator is used to detect the damage; however it was found to be a weak indicator of damage localization. A statistical decision making procedure is employed to determine the location of damage. The first step in this procedure is the selection of the maximum change in phase angle at each frequency value (the maximum value in each column of matrix [Π_r]) and discarding all other changes in phase angle measured at other nodes. For example in matrix [Π_r] (equation 3), if $\Delta_{3r}(f_1)$ is the maximum value in the first column then this value will be used as $B_{3r}(f_1)$ and other values in this column will be discarded. The same process is applied to the different columns in matrix [Π_r] to formulate the matrix of maximum changes of phase angle at different frequencies, [B_r]. It should be noted that [B_r] is a 3D matrix where each value of r ($r = 1 : n$) formulates one matrix

$$B_r = \begin{bmatrix} 0 & 0 & 0 & ..... & 0 \\ 0 & B_{2r}(f_2) & 0 & ..... & 0 \\ B_{3r}(f_1) & 0 & 0 & ..... & B_{3r}(f_m) \\ 0 & 0 & B_{4r}(f_3) & ..... & 0 \\ . & . & . & ..... & . \\ . & . & . & ..... & . \\ 0 & 0 & 0 & ..... & 0 \end{bmatrix}_r . \quad (5)$$

The total of maximum changes in phase angle is calculated from the sum of the rows of matrix [B_r] using different references. At each value of r, the sum of rows of matrix [B_r] will result in one vector. Therefore, n different vectors can be obtained. The sum of these vectors is stored in one vector {Z};

$$Z = \sum_r \begin{Bmatrix} \sum_f B_{1r}(f) \\ \sum_f B_{2r}(f) \\ \cdot \\ \cdot \\ \cdot \\ \sum_f B_{nr}(f) \end{Bmatrix}_r . \quad (6)$$

In order to monitor the frequency of damage detection at any node, a new matrix [E_r] is formulated. The matrix consists of 0's at the undamaged locations and 1's at the damaged locations. For example in the matrix [E_r] , we put a value of 1 corresponding to the locations of $B_{3r}(f_1)$, $B_{2r}(f_2)$ and so on, as shown in the following expression

$$E_r = \begin{bmatrix} 0 & 0 & 0 & ..... & 0 \\ 0 & 1 & 0 & ..... & 0 \\ 1 & 0 & 0 & ..... & 1 \\ 0 & 0 & 1 & ..... & 0 \\ . & . & . & ..... & . \\ . & . & . & ..... & . \\ 0 & 0 & 0 & ..... & 0 \end{bmatrix}_r . \quad (7)$$

Similar to the previous procedures, the total number of instances of detecting the damage at different nodes is calculated from matrix [E_r] as

$$K = \sum_r \begin{Bmatrix} \sum_f E_{1r}(f) \\ \sum_f E_{2r}(f) \\ \cdot \\ \cdot \\ \cdot \\ \sum_f E_{nr}(f) \end{Bmatrix}_r . \quad (8)$$

In order to reduce the effect of noise or measurement errors, a value of two times standard deviation of the elements in vector {K} will be subtracted from the vector {K}. Any resulting negative values will be removed. The same procedures is applied to the vector {Z} as follows

$$T = \begin{Bmatrix} Z_1 - 2\sigma \\ Z_2 - 2\sigma \\ \cdot \\ \cdot \\ \cdot \\ Z_n - 2\sigma \end{Bmatrix} \quad (9)$$

where $\sigma = \sqrt{\sum_{i=1}^{n} (Z_i - \bar{Z})^2} \Big/ (n-1)$, $\bar{Z} = \sum_{i=1}^{n} Z_i \Big/ n$,

$$I = \begin{Bmatrix} K_1 - 2\beta \\ K_2 - 2\beta \\ \cdot \\ \cdot \\ \cdot \\ K_n - 2\beta \end{Bmatrix} \quad (10)$$

where $\beta = \sqrt{\sum_{i=1}^{n} (K_i - \bar{K})^2} \Big/ (n-1)$, $\bar{K} = \sum_{i=1}^{n} K_i \Big/ n$.

The first damage location indicator is defined as the scalar product of { T } and { I } as shown in the following expression

$$Dam\_Ind\_1 = \begin{Bmatrix} T_1 \times I_1 \\ T_2 \times I_2 \\ \cdot \\ \cdot \\ \cdot \\ T_n \times I_n \end{Bmatrix} . \quad (11)$$

Another damage location indicator is formulated as follows:
The sum of rows of matrix $[B_r]$ (equation 5) at each reference channel represents a column in the following matrix

$$\Psi = \begin{bmatrix} \sum_f B_{11}(f) & \sum_f B_{12}(f) & ..... & \sum_f B_{1n}(f) \\ \sum_f B_{21}(f) & \sum_f B_{22}(f) & ..... & \sum_f B_{2n}(f) \\ . & . & ..... & . \\ . & . & ..... & . \\ . & . & ..... & . \\ \sum_f B_{n1}(f) & \sum_f B_{n2}(f) & ..... & \sum_f B_{nn}(f) \end{bmatrix} \quad (12)$$

where the first subscript represents the channel number and the second represents the reference number. A process of choosing the maximum value at each column and discarding other values of that column is used to construct the matrix Ψ_{max}.

$$\Psi_{max} = \begin{bmatrix} 0 & \sum_f B_{12}(f) & ..... & 0 \\ \sum_f B_{21}(f) & 0 & ..... & \sum_f B_{2n}(f) \\ . & . & ..... & . \\ . & . & ..... & . \\ . & . & ..... & . \\ 0 & 0 & ..... & 0 \end{bmatrix} \quad (13)$$

A new matrix [N] is constructed from 1's corresponding to the values in matrix Ψ_{max} and 0's at other locations as

$$N = \begin{bmatrix} 0 & 1 & . & . & . & 0 \\ 1 & 0 & . & . & . & 1 \\ . & . & . & . & . & . \\ . & . & . & . & . & . \\ . & . & . & . & . & . \\ 0 & 0 & . & . & . & 0 \end{bmatrix}. \quad (14)$$

The sum of rows of matrix $[\Psi_{max}]$ defines the vector $\{\Psi_{sum}\}$

$$\Psi_{sum} = \sum_r \Psi_{max}, \quad (15)$$

and the sum of rows of matrix N defines the vector $\{N_{sum}\}$

$$N_{sum} = \sum_r N. \quad (16)$$

Then the second damage location indicator is defined as the scalar product of vectors $\{\Psi_{sum}\}$ and $\{N_{sum}\}$

$$Dam\_Ind\_2 = \Psi_{sum} . \times N_{sum}. \quad (17)$$

Damage indicators 1 and 2 will be used to determine the damage location. On the other hand, the total change in phase angle (equation 4) will be used to detect the occurrence of damage and assess the damage extent.

3. Steel bridge model

3.1 Experimental setup and equipment

In this research, a steel bridge model is examined after inducing damage with different levels to some members. The model consists of two girders and six cross beams. Each cross beam is connected to the girders with four bolts, 2 bolts in each side. The model dimensions and layout are shown in Figures 1 and 2. The multi-layer piezoelectric actuator is used for local excitation. The main advantage of using piezoelectric actuator is that it produces vibration with different frequencies ranging from 0.1 to 400 Hz that is effective in exciting different mode shapes[8, 9]. Five natural frequencies are measured in the range of the excitation frequency (from 0.1 to 400 Hz) at 43.75, 118.85, 212.5, 300, 393.75 Hz. The actuator force amplitude is 0.2 kN. The actuator is located at the center of the upper flange of the main girder (Figures 1 and 2). The location of the actuator is not changed during different damage states of the structure. The effects of changing the actuator location on the accuracy of the results are not studied in this research. The excitation forces used for the undamaged and damaged structure are uniform (the frequency of the input force gradually increase from 0.1 to 400 Hz), equal in amplitude (the maximum force magnitude that the actuator can provide equals 0.2 kN) and have the same vibration waveform (sinusoidal sweep functions). The actuator is pressured to the structure by a spring but is not glued to the structure's surface. Therefore, the actuator always provides pressure forces and cannot provide tension forces. The excitation force was not measured however, it can be simulated as shown in Figure 3. One accelerometer is mounted at the bottom of each cross beam to measure the acceleration response in the vertical direction at the mid span of each cross beam, as shown in Figure 2. Each time signal was sampled at 1600 Hz Main characteristics of the equipments used in this experiment are shown in Table 1. Four cases of damage are introduced to the specimen as follows:

Case 1: Removing one bolt completely from the left side of cross beam no. 2 (Figure 4).

Case 2: Case 1 + releasing one bolt at the left side of cross beam no. 2 (Figure 4).

Case 3: Case 2 + removing one bolt at the right side of cross beam no. 2 (Figure 4).

Case 4: Removing one bolt and releasing the second one from the left side of cross beam no. 2. The same damage is introduced to cross beam no. 5.

3.2 Damage identification algorithm applied to different damage cases for the steel bridge model

(1) Cases 1, 2 and 3 (damage at beam no. 2)

CSD is calculated from node point accelerations between each measuring channel and a reference channel using MATLAB[23, 24] standard and the MATLAB Signal Processing Toolbox. Then the phase angle is calculated from the real and imaginary values of CSD data. Every measuring channel will be used once as a reference for other channels and so on. The phase angle is measured in the frequency range of 1–800 Hz. This range is determined based only on the sampling rate of collecting the data rather than the frequency content of the excitation force. Hanning window of size 256 is applied to the time signals to minimize leakage. In this technique, the

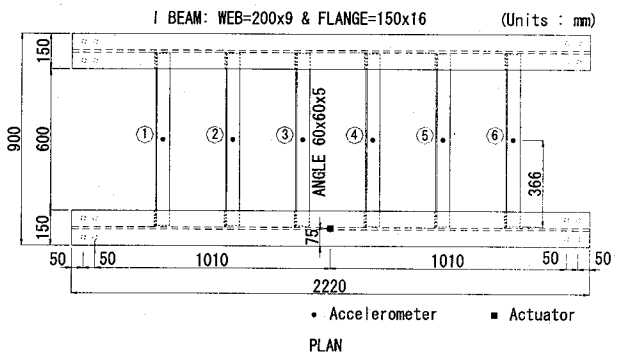

Figure 1 Basic dimensions of the bridge model and beam numbers

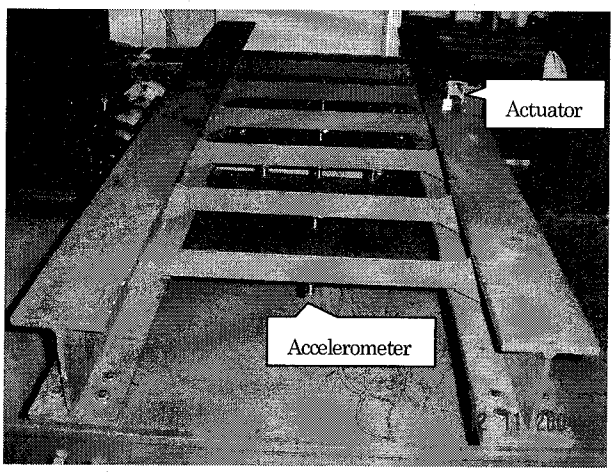

Figure 2 Accelerometers and actuator positions

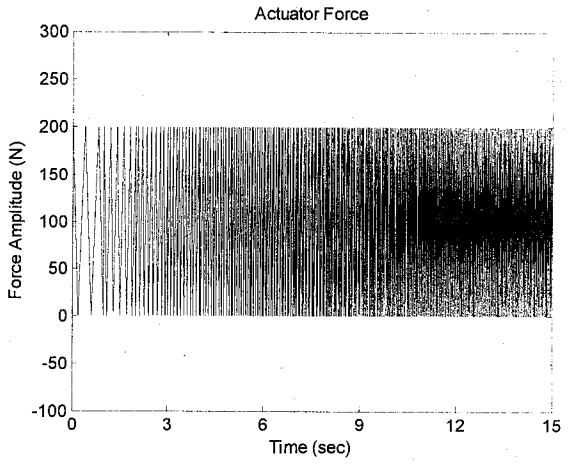

Figure 3 Simulation of the actuator force

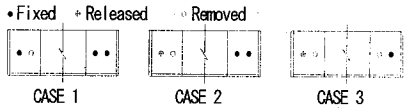

Figure 4 Damage cases introduced to cross beam no. 2

signal (acceleration data) is divided into overlapping sections of the specified window length (256) and windows each section using the Hanning window function. Phase angle values in the frequency range of 10–800 Hz are used for the proposed method. This frequency

Table 1 Equipment characteristics

Piezoelectric actuator	
Dimensions (W×T×H)	10×10×20 (mm)
Min. and Max freq.	0~982 Hz
Displacement (100V)	12.3 μm
Piezoelectric accelerometer	
Dimensions (Base×H)	17 Hex × 32 (mm)
Frequency Bandwidth	5~4000 Hz
Sensitivity	10 mV/(m/s^2)

range covers most of the measured range (1–800 Hz). Only a small range of 1–10 Hz is not used to avoid the low frequency noise. In case of using a Hanning window size of 256, the phase angle is measured at 129 frequency lines (frequency step = 800*2/256). Thus, the frequency range from 1–10 Hz contains one frequency line only and represents 1.25% of the total measurement range. It was noticed that excluding a small range of measurement (1–2% of the total measurement range) from the beginning and the end of the total measurement range sometimes improves the accuracy of the obtained results. However, it is not always needed to eliminate a small range from the measurement and the accuracy of the results will not significantly be affected. It was decided to use phase angle data in the measurement range (10–800 Hz) beyond the actuator capacity (0.1–400 Hz) based only on the sampling rate of collecting the data. It is desirable to use phase angle data in the total measurement range to avoid the problem of determining the best frequency range in which phase angle has to be measured. In other words, phase angle data can be used in the total measured frequency range regardless of the frequency content of the excitation force and without the need to identify the best frequency range in which the phase angle has to be used. The experiment was repeated four times on the undamaged structure without any change in the experimental setup. Figure 5 shows the phase angle between channel 2 and channel 5 for two different sets of data obtained from the undamaged structure. Some changes in phase angle data can be observed in this figure before introducing any damage to the structure. These changes are small and obviously due to noise and measurement errors contained on the data. The total change in phase angle at each channel, measured in a certain frequency range, can be determined using equation (4). The total change in phase angle for two sets of data obtained from the undamaged structure is shown in Figure 6. As clearly indicated in this figure, the total change in phase angle ranges from about 150 to 220 radian with close values at different channels. When the total change in phase angle was calculated for another two sets of data obtained from the undamaged structure, similar results were obtained. In a similar manner, the total change in phase angle that results from environmental changes or operational loads can be estimated at each measuring channel. Thus, a threshold of the total change in phase angle that results from noise, measurement errors, environmental changes or operational loads can be estimated at each measuring channel. It is assumed that damage will produce greater values of the total change in phase angle than the estimated threshold values. Therefore, the total change in phase angle will be used for detecting

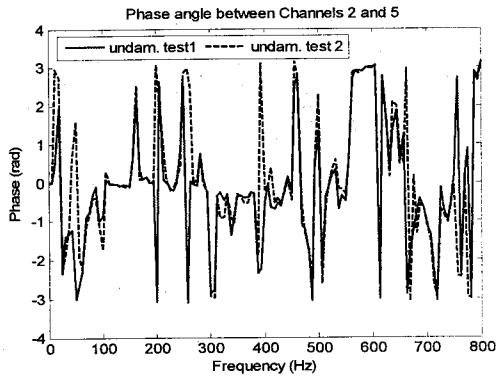

Figure 5 Phase angle for two sets of data obtained from the undamaged structure

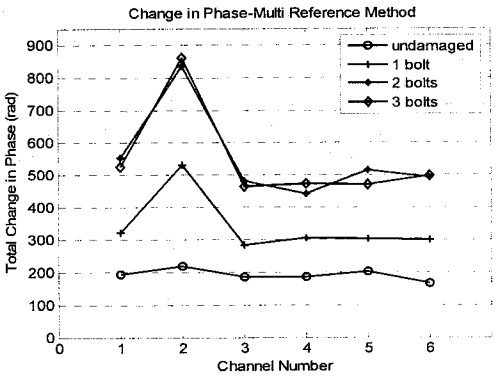

Figure 7 Total change in phase angle for different damage cases

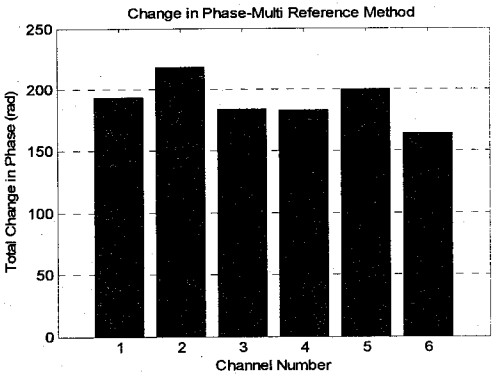

Figure 6 Total change in phase angle due to noise

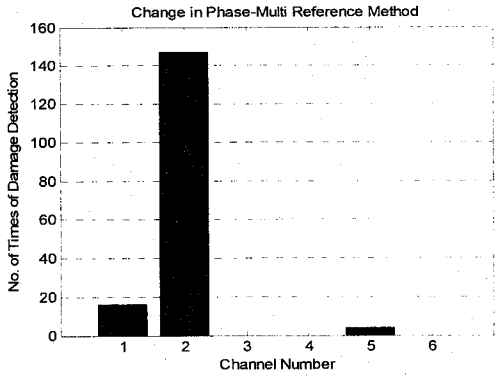

Figure 8 Number of times of detecting damage at channel 2 for damage case 1

the occurrence of damage in the structure. On the other hand, it was found to be a weak indictor of identifying damage location. Figure 7 shows the total change in phase angle for the following cases: (i) two undamaged cases indicated by the legend undamaged, (ii) the undamaged structure and damage case 1 indicated by the legend 1 bolt, (iii) the undamaged structure and damage case 2 indicated by the legend 2 bolts and (iv) the undamaged structure and damage case 3 indicated by the legend 3 bolts. The following remarks can be drawn from this figure:

- The total change in phase angle values increased at all channels after introducing the first level of damage. The total change at the damaged location (channel 2) is bigger than that at the undamaged locations.
- As the damage level increases in damage case 2, the same previous remarks are also observed.
- No significant changes are observed between damage cases 2 and 3 since the beam had already lost most of its stiffness in case 2.
- Peak value at channel 2 can indicate the damage location however damage indicators 1 and 2 were found to be better indictors of damage location than using the total change in phase angle as will be illustrated in the following sections.

The results of damage location for damage case 1, using damage indicators 1 (equation 11) and 2 (equation 17), are shown in Figures 8-10. Figure 8 shows the number of times of detecting the damage at each channel using equation (10). Damage at channel 2 (the damaged location) is detected 147 times compared to 16 times at channel 1, and 4 times at channel 5 (undamaged locations). The number of times of detecting the damage at the correct location is usually much higher than that at the undamaged locations (false positive readings). Therefore, multiplying the number of times of detecting the damage at each channel to the change in phase angle at the same channel will increase the value of the damage indicator at the damage locations and reduce its value at the undamaged locations (equation 11). Damage location is determined very accurately at channel 2 using both damage indicators 1 and 2 (Figures 9 and 10). A false positive reading appeared at channel 3 (Figure 10); however the damage indicator value at this channel is very small compared to its value at the correct damage location.

(2) Case 4 (damage at beams no. 2 and 5)

In case 4, similar damage is introduced to beams no. 2 and 5 simultaneously. Damage indicator 1 determined the damage locations at channels 2 and 5 accurately, as shown in Figure 11. However, small false positive readings appeared at channels 1 and 6. Damage indicator 2 determined damage locations at channel 2 and 5 accurately. On the other hand, damage at beam no. 5 is detected with relatively smaller damage indicator value (Figure 12). Moreover one false positive reading appeared at channel 1. The previous results were obtained using Hanning window of size 256. When the

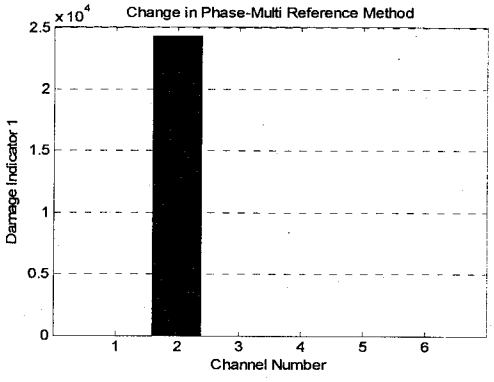

Figure 9 Damage localization results for damage case 1 using damage indicator 1

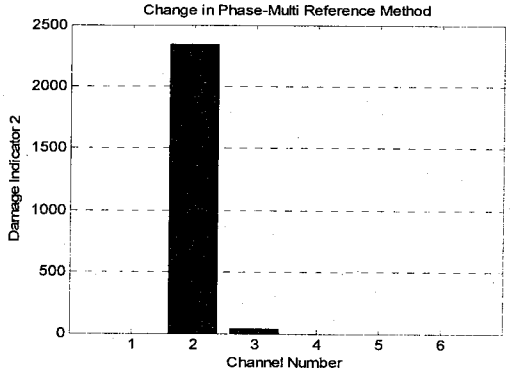

Figure 10 Damage localization results for damage case 1 using damage indicator 2

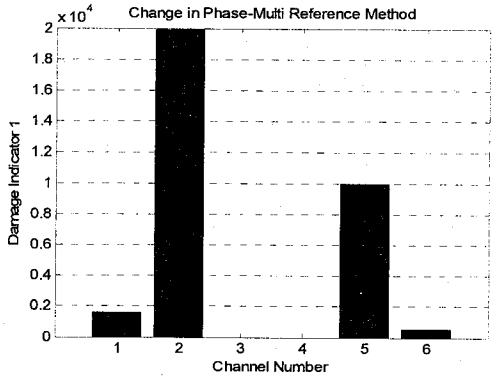

Figure 11 Damage localization results for damage case 4 using damage indicator 1 (window size = 256)

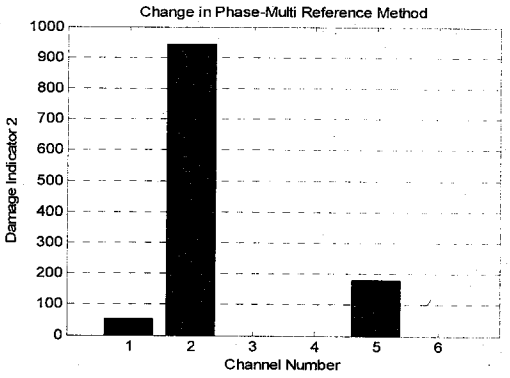

Figure 12 Damage localization results for damage case 4 using damage indicator 2 (window size = 256)

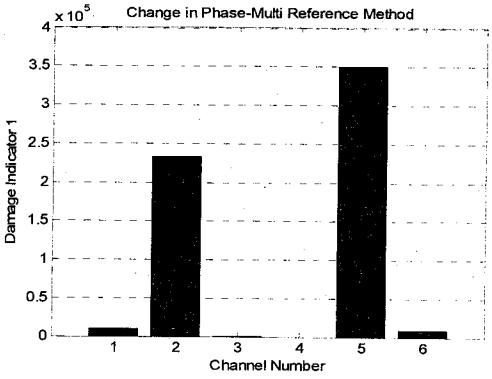

Figure 13 Damage localization results for damage case 4 using damage indicator 1 (window size = 1024)

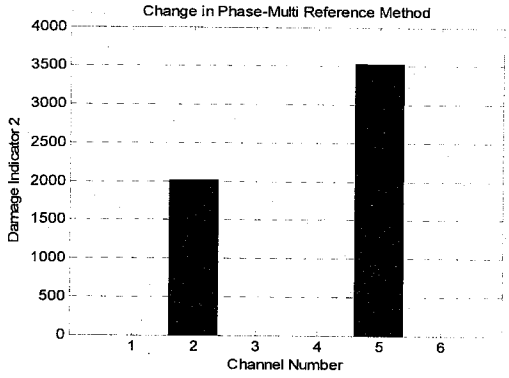

Figure 14 Damage localization results for damage case 4 using damage indicator 2 (window size = 1024)

Hanning window size increased to 1024 better results were obtained for both damage indicators, as shown in Figures 13 and 14.

4. Bookshelf structure

For further validation of the proposed method, it is also applied to the experimental data from a bookshelf structure. The experimental work on the bookshelf structure was done by Charles R. Farrar and David V. Jauregui of Los Alamos National Laboratory (LANL), U.S.A[25]. The tested structure is a three-story frame structure model as shown in Figure 15. It is constructed of aluminum columns and aluminum floor plates. The floors are 1.3 cm thick aluminum plates with two-bolt connections to brackets on the column. The base is a 3.8 cm thick aluminum plate. Support brackets for the columns are bolted to this plate and hold the columns. Dimensions of the test structure are displayed in Figures 16 and 17. All bolted connections are tightened to a torque of 6.77 N.m in the undamaged state. Four air mount isolators, which allow the structure to move freely in horizontal directions, are bolted to the bottom of the base plate. The isolators are inflated to 140 kPa gauge and then adjusted to allow the

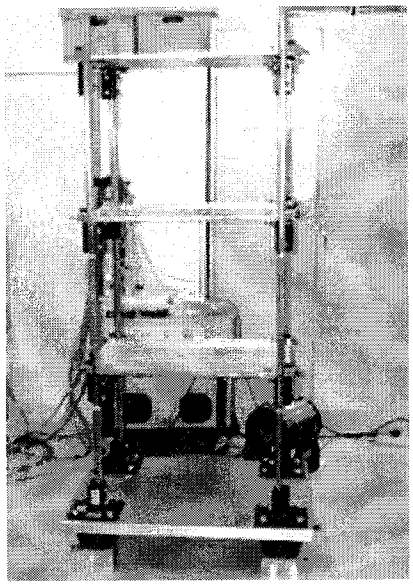

Figure 15 Photo of the full test structure

Table 2 Channel position

Ch.	Posit.
1	3BP
2	3BC
3	3AP
4	3AC
5	3CP
6	3CC
7	3DP
8	3DC
9	2BP
10	2BC
11	2AP
12	2AC
13	2CP
14	2CC
15	2DP
16	2DC
17	1BP
18	1BC
19	1AP
20	1AC
21	1CP
22	1CC
23	1DP
24	1DC

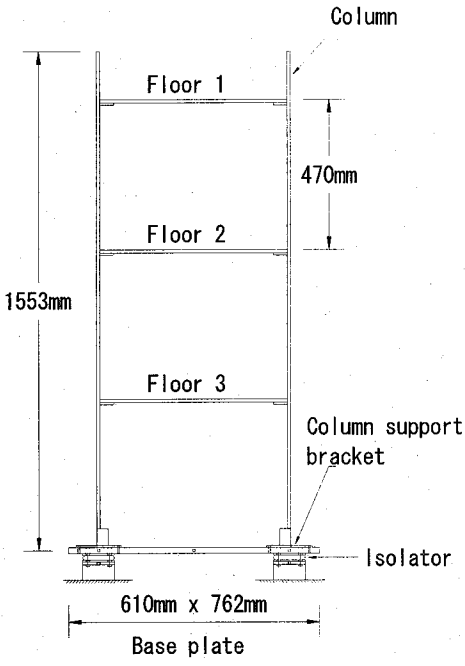

Figure 16 Basic dimensions of the 3 story frame structure

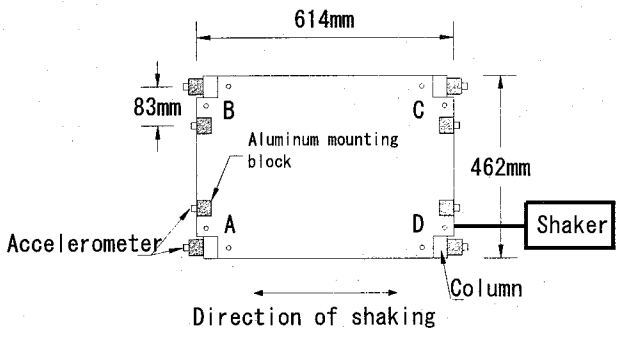

Figure 17 Floor layout as viewed from above

structure to sit at the same level with the shaker. The isolators were needed to allow the shaker to push and pull the structure without strong resistance and to provide more flexibility to the structure to move in horizontal directions. However, it was not intended to use the isolators to reduce the effect of ambient vibration. The shaker is coupled to the structure by a 15 cm long, 9.5-mm diameter stinger connected to a tapped hole at the mid-height of the base plate. The shaker is attached at corner D (shifted from the centerline of the base plate) as shown in Figure 17, so that the base plate will move in horizontal directions (translational motion) and will also rotate in the horizontal plane around its center of gravity (torsional motion). Thus, both translational and torsional motions can be excited.

4.1 Test setup and data acquisition

The structure is instrumented with 24 piezoelectric single axis accelerometers, two per joint as shown in Figure 17. Accelerometers are mounted on the aluminum blocks that are attached by hot glue to the plate and column. This configuration allows relative motion between the column and the floor to be detected. The nominal sensitivity of each accelerometer is 1 V/g. A commercial data acquisition system controlled from a laptop PC is used to digitize the accelerometer analog signals. The data sets that were analyzed in the feature extraction and statistical modeling portion of the study were the acceleration time histories. In the damaged cases, the bolts at the joint indicated were loosened and then tightened again to hand tight allowing the plate to move relative to the column. All input from the shaker to the base was random. In each test case, the data sets were collected with the shaker input level kept at 8 volts. The bandwidth of the shaker and response were also kept at equal values for different test cases. Each time signal gathered consisted of 8192 points and were sampled at 1600 Hz. Figure 18 shows the transfer function estimate between the acceleration response at channel 15 and the excitation force. As clearly indicated in this figure, considerable number of modes could be excited in the frequency range from 1–800 Hz. Channels 1-24 represent the accelerometers placed on the structure. Channels 1 and 2 represent the first pair of sensors across a joint, 3 and 4 are the next and so on. Each sensor position is marked with either a P (Plate) or C (column) to indicate the position relative to the joint. Channel number and the corresponding position are shown

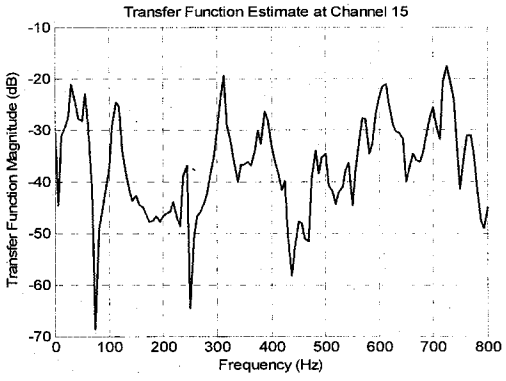

Figure 18 Transfer function estimate at channel 15

in Table 2. The following damage cases are introduced to the bookshelf structure:

Case 1: Damage location is 1C (floor 1, corner C). The bolts between the bracket and the plate are left in at a torque value of 1.128 N.m.

Case 2: Damage location is 1C (floor 1, corner C). The bolts between the bracket and the plate are left in at a torque value of 0.564 N.m.

Case 3: Damage location is 3A (floor 3, corner A). The bracket is completely removed.

Case 4: Damage locations are 3A and 1C. The bolts are removed between the bracket and the plate at both damage locations.

4.2 Damage identification algorithm applied to different damage cases for the bookshelf structure

(1) Cases 1 and 2 (channels 21 and 22)

In cases 1 and 2, damage location exists at corner C in floor 1. Therefore channels 21 and 22 are the nearest channels to the damage location, as shown in Table 2. Figure 19 shows the total change in phase angle for the following cases: (i) two sets of data obtained from the undamaged structure indicated by the legend undamaged, (ii) the undamaged structure and damage case 1 indicated by the legend damage 1, and (iii) the undamaged structure and damage case 2 indicated by the legend damage 2. Before introducing any damage to the structure, the total changes in phase angle at different channel are similar and exist around the value of 500 radian. After introducing the first level of damage at location 1C, the total change in phase angle increased at all channels to the values above 2000 radian with a bigger change at channel 22 (damage location). No significant changes were observed in the total change of phase angle after increasing the damage at location 1C. Therefore, it can be concluded that the total change in phase angle is a useful tool to detect the occurrence of damage but it cannot be used to estimate the severity of damage. Damage localization results using damage indicators 1 and 2 are shown in Figures 20 and 21, respectively. Both damage indicators determined the damage location at channel 22 very accurately. Only one very small false positive reading appeared at channel 17 when damage indicator 1 was used.

(2) Case 3 (channels 3 and 4)

Damage location is changed in case 3 to examine the feasibility of the proposed method to detect and locate the damage at different locations. In this case, damage exists at corner A in floor 3 (Figures 16 and 17). Therefore, channels 3 and 4 are the nearest channels to the damage location (Table 2). Damage indicator 1 determined the damage location accurately at channel 3 with a smaller indication at channel 4, as shown in Figure 22. Two small false positive readings appeared at channels 8 and 16. Damage indicator 2 determined the damage location at channel 3 without any false positive readings (Figure 23). Damage indicator 2 determined the damage location in this case and the previous case more accurately than damage indicator 1. However, damage indicator 1 showed better results in some cases of the bridge model. Therefore, it is necessary to use both damage indicators to confirm the right location of damage.

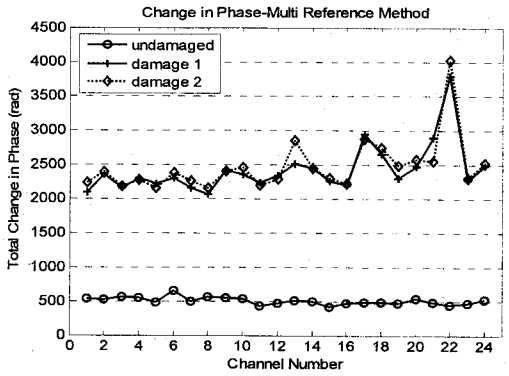

Figure 19 Total change in phase angle for different damage cases

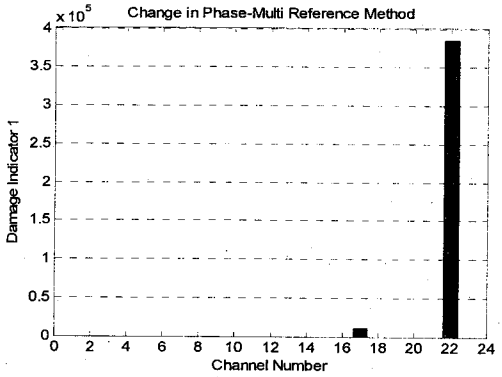

Figure 20 Damage localization results for damage case 1 using damage indicator 1

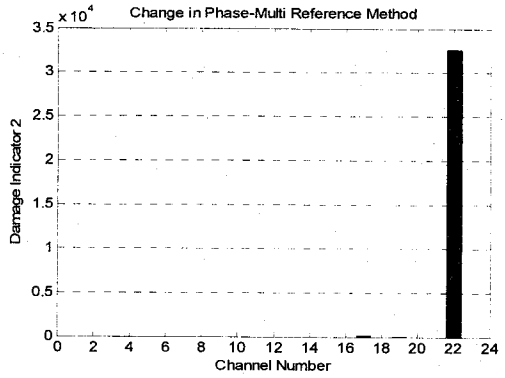

Figure 21 Damage localization results for damage case 1 using damage indicator 2

(3) Case 4 (channels 3, 4, 21 and 22)

In case 4, the same damage is introduced to two locations; corner C, floor 1 (near to channel 21 and 22) and corner A, floor 1 (near to channel 3 and 4). Both damage indicators 1 and 2 determined the damage at the two locations accurately without any false positive readings, as shown in Figures 24 and 25. Damage indicator value at channel 4 is smaller than that at channel 22 although the damage level is the same at the two locations. This is because the amount of noise or measurement errors is not the same at different measuring

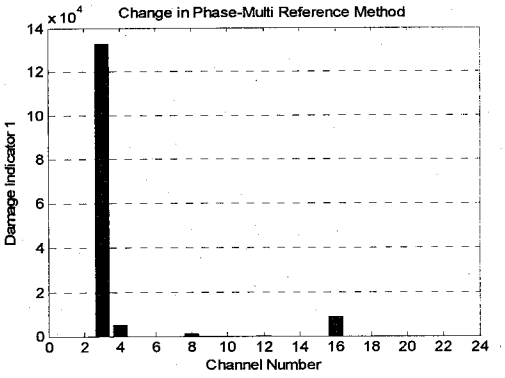

Figure 22 Damage localization results for damage case 3 using damage indicator 1

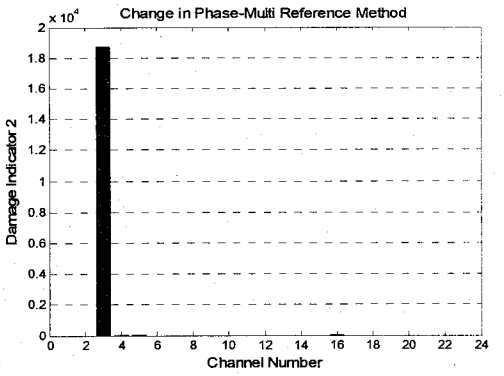

Figure 23 Damage localization results for damage case 3 using damage indicator 2

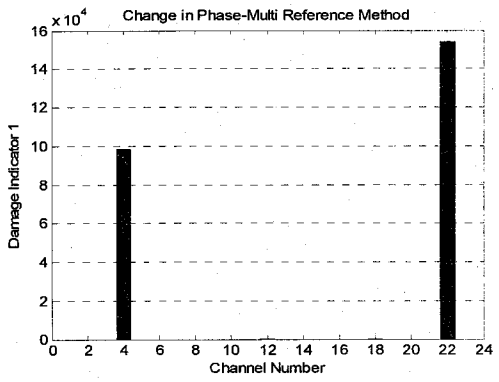

Figure 24 Damage localization results for damage case 4 using damage indicator 1

channels. Moreover, the level of excitation and mode shape values are different at different locations.

5. Conclusions

A damage detection experimental study using a steel bridge model and bookshelf structure was presented. The methodology can be applied in a similar manner to large civil engineering structures, such as steel bridges. For example, a number of sensors can be mounted on the main girder of the bridge and a number of actuators

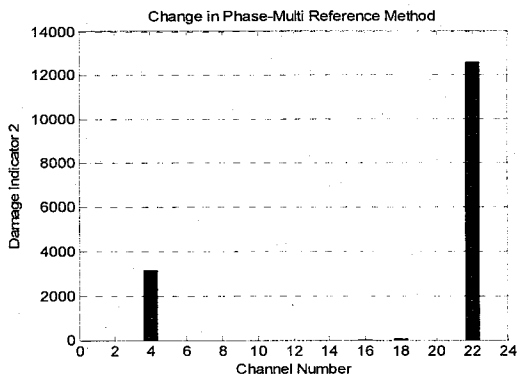

Figure 25 Damage localization results for damage case 4 using damage indicator 2

can be used as a local excitation source for the main girder. In such case, the monitored structural element can be excited to a high frequency range using the actuators. The same excitation force (equal magnitude and the same waveform) can be produced for exciting the undamaged and damaged structure as required to implement the damage identification technique presented in this paper. Undesired vibrations induced from wind, traffic or any other source can be avoided since the vibration data induced from the actuators can be generated at any desired time. Moreover, the traffic over the bridge does not need to be interrupted.

The proposed approach is a global NDE method which uses vibration measurements and, therefore, is limited to identifying structural damages that produce measurable changes in the structural dynamic characteristics. The excitation forces used for the undamaged and damaged structure must have the same amplitude, location and waveform in order to ensure that the changes in phase angle data are mainly due to damage and not due to the change in excitation force characteristics. The excitation force does not need to be measured and no structural model is needed. The proposed method detected the damage and determined its location accurately for most of damage cases that were introduced to the test structures. Single and double damage were introduced to the test structures; however the application of the proposed method to the case of multiple-damage needs to be studied. It was also observed that the method gives better results in case of single damage than the case of double damage. The method can be used to detect the damage and locate its position but it cannot be used to estimate the severity of damage. The proposed algorithm uses the measured phase angle in a certain frequency range without the need for any modal data. The phase angle can be used in the total measured frequency range without the need to determine the best frequency range that gives the most accurate results.

Acknowledgement

This research is supported by the Grant-in-Aids for Scientific Research, Ministry of Education. The authors wish to express their gratitude for this support. The authors would like to acknowledge Dr.

Farrar and LANL for the authorization in using the photos, drawings and data of the bookshelf structure.

References

1) Rubin S. Ambient vibration survey of offshore platform. ASCE J. Engng Mech Div 1980;106(3):425-41.
2) Hyoung M. Kim, Theodore J. Bartkowicz, An experimental study for damage detection using a hexagonal truss, *J. Computers and Structures 79 (2001) 173-182.*
3) Park, S., Stubbs, N. and Bolton, R.W., Damage Detection on a Steel Frame Using Simulated Modal Data, *16th International Modal Analysis Conference (IMAC XVI)*, Santa Barbara, California, February 2-5, Proceedings, pp. 612–622, 1998.
4) Kim J. - T., and Stubbs N., Crack Detection in Beam-Type Structures Using Frequency Data, *Journal of Sound and Vibration*, 259(1), 145–160, Williamsburg, VA, 2003.
5) Ewins D. J., *Modal Testing: Theory and Practice*, John Wiley, New York, 1985.
6) Abdo M. A.-B. and Hori M., A Numerical Study of Structural Damage Detection Using Changes In The Rotation of Mode Shapes, *Journal of Sound and Vibration*, 251(2), pp. 227-239, 2002.
7) Farrar C. R. and D. A. Jauregui, *Damage Detection Algorithms Applied to Experimental and Numerical Model Data from the I-40 Bridge*, Los Alamos National Laboratory Report, LA-12979-MS, 1996.
8) Oshima T. et al., Study on damage evaluation of joint in steel member by using local vibration excitation, (In Japanese), *Journal of Applied Mechanics JSCE*, Vol.5, pp.837-846, 2002.
9) Beskhyroun S., Oshima T., Mikami S., Yamazaki T., Damage detection and localization on structural connections using vibration based damage identification methods, *Journal of Applied Mechanics, JSCE*, Vol.6, pp. 1055-1064, 2003.
10) Doebling S. W., C. R. Farrar, M. B. Prime, and D. W. Shevitz, *Damage Identification and Health Monitoring of Structural and Mechanical Systems from Changes in their Vibration Characteristics*, A Literature Review, Los Alamos National Laboratory Report, LA-13070- MS, 1996.
11) Farrar C. R. and D. A. Jauregui, *Damage Detection Algorithms Applied to Experimental and Numerical Model Data from the I-40 Bridge*, Los Alamos National Laboratory Report, LA-12979-MS, 1996b.
12) Sampaio R. P. C., Maia N. M. M. and Silva J. M. M., Damage detection using the frequency-response-function curvature method, *Journal of Sound and Vibration*, 226(5), pp. 1029-1042, 1999.
13) Ojalvo, I.U., and Pilon, D., Diagnostics for Geometrically Locating Structural Math Model Errors from Modal Test Data, *Proc. of 29th AIAA/ASME/ASCE/ASC Structures, Structural Dynamics, and Materials Conference*, Williamsburg, VA, 1988.
14) Ricles, J.M., and Kosmatka, J.B., Damage Detection in Elastic Structures Using Vibratory Residual Forces and Weighted Sensitivity, *AIAA Journal*, Vol. 30, No. 9, pp. 2310-2316, 1992.
15) Smith, S.W., and Li, C., A Hybrid Approach for Damage Detection in Flexible Structures, *Proceedings of the 35th AIAA/ASME/ASCE/AHS/ASC Structures, Structural Dynamics, and Materials Conference*, pp. 285-293, AIAA-94-1710-CP, 1994.
16) Carrasco, C.J. Osegueda, R.A. and Ferregut, C.M, *Modal Tests of a Space Truss Model and Damage Localization Using Modal Strain Energy*, Report FAST 96-10 - FAST Center for Structural
17) Peeters B., Maeck J. and De Roeck G., Vibration-based damage detection in civil engineering: excitation sources and temperature effects, *Smart Materials and Structures*, 10, pp.518-527, 2001.
18) Kummer E., Yang J. C. S. and Dagalakis N. G., Detection of fatigue cracks in structural members, *2nd American Society of Civil Engineering/EMD Specialty Conference*, Atlanta, Georgia, 445-460, 1981.
19) Yang J. C. S., Chen J. and Dagalakis N. G., Damage detection in offshore structures by the random decrement technique, *Journal of Energy Resources Technology*, American Society of Mechanical Engineers 106, 38-42, 1984.
20) Flesch R. G. and Kernichler K., Bridge inspection by dynamic tests and calculations dynamic investigations of Lavent bridge, *workshop on Structural Safety Evaluation Based on System Identification Approaches* (H. G. Natke and J. T. P. Yao, editors), 433-459, Lambrecht/ Pfalz, Germany: Vieweg & Sons, 1988.
21) Masri S. F., Miller R. K., Saud A. F. and Caughey T. K., Identification of nonlinear vibrating structures, *Journal of Applied Mechanics 54*, 923-929: Part I-formulation, 1987.
22) Natke H. G. and Yao J. T. P., System identification methods for fault detection and diagnosis, *International Conference on Structural Safety and Reliability*, American Society of Civil Engineers, New York, 1387-1393, 1990.
23) MATLAB Reference Guide, The Math Works, Inc., Natick, MA, 2003.
24) MATLAB User's Guide, The Math Works, Inc., Natick, MA, 2003.
25) [www http://ext.lanl.gov/projects/damage_id/data.htm].

(Received: September 10, 2005)